

University of Groningen

## Optimisation of scan duration and image quality in oncological <sup>89</sup>Zr immunoPET imaging using the Biograph Vision PET/CT.

van Sluis, Joyce; Boellaard, Ronald; Dierckx, Rudi A J O; van Esch, Evelien L M; Croes, Demi A; de Ruijter, Laura Kist; van de Donk, Pim P; de Vries, Elisabeth G E; Noordzij, Walter; Brouwers, Adrienne H

*Published in:*

European Journal of Nuclear Medicine and Molecular Imaging

*DOI:*

[10.1007/s00259-023-06194-4](https://doi.org/10.1007/s00259-023-06194-4)

**IMPORTANT NOTE: You are advised to consult the publisher's version (publisher's PDF) if you wish to cite from it. Please check the document version below.**

*Document Version*

Publisher's PDF, also known as Version of record

*Publication date:*  
2023

[Link to publication in University of Groningen/UMCG research database](#)

*Citation for published version (APA):*

van Sluis, J., Boellaard, R., Dierckx, R. A. J. O., van Esch, E. L. M., Croes, D. A., de Ruijter, L. K., van de Donk, P. P., de Vries, E. G. E., Noordzij, W., & Brouwers, A. H. (2023). Optimisation of scan duration and image quality in oncological <sup>89</sup>Zr immunoPET imaging using the Biograph Vision PET/CT. *European Journal of Nuclear Medicine and Molecular Imaging*, 50, 2258–2270. Advance online publication. <https://doi.org/10.1007/s00259-023-06194-4>

### Copyright

Other than for strictly personal use, it is not permitted to download or to forward/distribute the text or part of it without the consent of the author(s) and/or copyright holder(s), unless the work is under an open content license (like Creative Commons).

The publication may also be distributed here under the terms of Article 25fa of the Dutch Copyright Act, indicated by the "Taverne" license. More information can be found on the University of Groningen website: <https://www.rug.nl/library/open-access/self-archiving-pure/taverne-amendment>.

### Take-down policy

If you believe that this document breaches copyright please contact us providing details, and we will remove access to the work immediately and investigate your claim.



# Optimisation of scan duration and image quality in oncological $^{89}\text{Zr}$ immunoPET imaging using the Biograph Vision PET/CT

Joyce van Sluis<sup>1</sup> · Ronald Boellaard<sup>1,2</sup> · Rudi A. J. O. Dierckx<sup>1</sup> · Evelien L. M. van Esch<sup>1</sup> · Demi A. Croes<sup>1</sup> · Laura Kist de Ruijter<sup>3</sup> · Pim P. van de Donk<sup>3</sup> · Elisabeth G. E. de Vries<sup>3</sup> · Walter Noordzij<sup>1</sup> · Adrienne H. Brouwers<sup>1</sup>

Received: 22 December 2022 / Accepted: 7 March 2023 / Published online: 22 March 2023  
© The Author(s) 2023

## Abstract

**Purpose** Monoclonal antibody (mAb)-based PET (immunoPET) imaging can characterise tumour lesions non-invasively. It may be a valuable tool to determine which patients may benefit from treatment with a specific monoclonal antibody (mAb) and evaluate treatment response. For  $^{89}\text{Zr}$  immunoPET imaging, higher sensitivity of state-of-the-art PET/CT systems equipped with silicon photomultiplier (SiPM)-based detector elements may be beneficial as the low positron abundance of  $^{89}\text{Zr}$  causes a low signal-to-noise level. Moreover, the long physical half-life limits the amount of activity that can be administered to the patients leading to poor image quality even when using long scan durations. Here, we investigated the difference in semiquantitative performance between the PMT-based Biograph mCT, our clinical reference system, and the SiPM-based Biograph Vision PET/CT in  $^{89}\text{Zr}$  immunoPET imaging. Furthermore, the effects of scan duration reduction using the Vision on semiquantitative imaging parameters and its influence on image quality assessment were evaluated.

**Methods** Data were acquired on day 4 post 37 MBq  $^{89}\text{Zr}$ -labelled mAb injection. Five patients underwent a double scan protocol on both systems. Ten patients were scanned only on the Vision. For PET image reconstruction, three protocols were used, i.e. one camera-dependent protocol and European Association of Nuclear Medicine Research Limited (EARL) standards 1 and 2 compliant protocols. Vision data were acquired in listmode and were reprocessed to obtain images at shorter scan durations. Semiquantitative PET image parameters were derived from tumour lesions and healthy tissues to assess differences between systems and scan durations. Differently reconstructed images obtained using the Vision were visually scored regarding image quality by two nuclear medicine physicians.

**Results** When images were reconstructed using 100% acquisition time on both systems following EARL standard 1 compliant reconstruction protocols, results regarding semiquantification were comparable. For Vision data, reconstructed images that conform to EARL1 standards still resulted in comparable semiquantification at shorter scan durations (75% and 50%) regarding 100% acquisition time.

**Conclusion** Scan duration of  $^{89}\text{Zr}$  immunoPET imaging using the Vision can be decreased up to 50% compared with using the mCT while maintaining image quality using the EARL1 compliant reconstruction protocol.

**Keywords** Zirconium-89 · ImmunoPET · SiPM · Image quality · Scan time

This article is part of the Topical Collection on Oncology - General.

✉ Joyce van Sluis  
j.van.sluis@umcg.nl

<sup>1</sup> Department of Nuclear Medicine and Molecular Imaging, University Medical Center Groningen, University of Groningen, Hanzeplein 1, 9713 GZ Groningen, The Netherlands

<sup>2</sup> Department of Radiology and Nuclear Medicine, University Medical Centers Amsterdam, Free University of Amsterdam, De Boelelaan 1117, 1081 HV Amsterdam, The Netherlands

<sup>3</sup> Department of Medical Oncology, University Medical Center Groningen, University of Groningen, Hanzeplein 1, 9713 GZ Groningen, The Netherlands

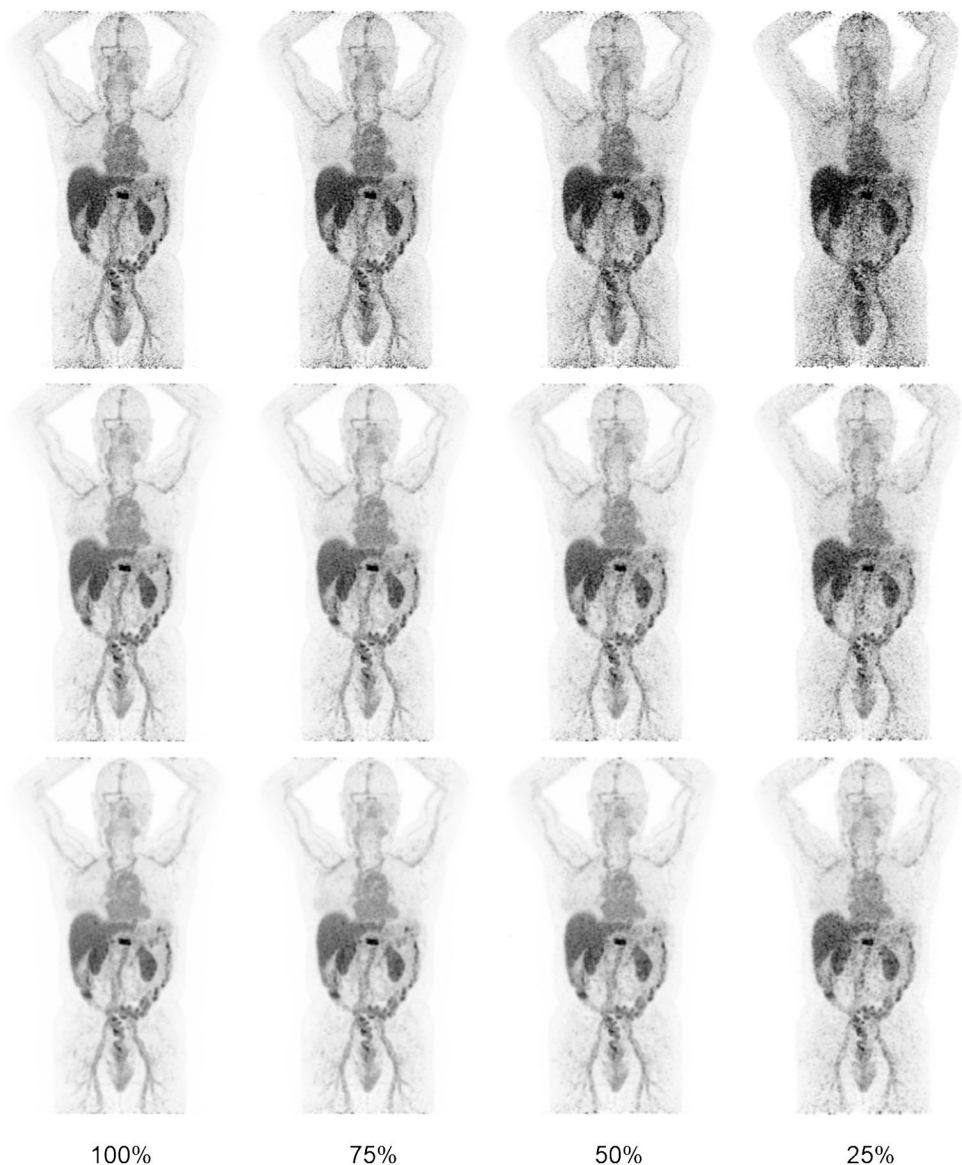
## Introduction

The latest generation positron emission tomography (PET) integrated with computed tomography (CT) systems is equipped with silicon photomultiplier (SiPM)-based detector elements. These systems with improved detection capabilities may contribute to enhance diagnostic performance [1–3], but could also allow a reduction in scan duration and/or reduction in administered radioactivity [3, 4].

Over the past decades, antibody-based PET (immunoPET) imaging has become increasingly important in drug development [5]. In addition, it may be a valuable tool to determine which patients may benefit from treatment with a specific monoclonal antibody (mAb) via non-invasive characterisation of tumour lesions, and for evaluation of treatment response [6].

Numerous advantages of zirconium-89 ( $^{89}\text{Zr}$ ), such as the long half-life of 78.4 h matching the pharmacokinetic behaviour of antibodies, its relatively low average positron energy of 395 keV resulting in low positron range (3.6 mm in water) for high-resolution PET imaging, and good in vivo stability, make it a suitable candidate for labelling of mAb [7–9]. For  $^{89}\text{Zr}$  immunoPET imaging, the higher sensitivity of SiPM-based PET/CT systems could be particularly beneficial as the low positron abundance (22.7%) causes the acquired PET images to have a low signal-to-noise level. In addition, the high-energy gamma emission of 909 keV causes high radiation burden and limits the amount of radiotracer that can be administered to patients [10]. Hence, long scan durations are required to obtain adequate statistical image quality, especially at later scan time points.

**Fig. 1** Patient example  $^{89}\text{Zr}$  immunoPET images obtained using the Vision PET/CT. Maximum intensity projection PET images acquired at day 4 p.i. of 37 MBq [ $^{89}\text{Zr}$ ]mAb of a 79-year-old patient (weight 86 kg) with metastatic breast cancer acquired at 100%, 75%, 50% and 25% of the scan duration (from left to right, respectively) using the Clinical Vision, EARL2 Vision and EARL1 Vision reconstruction protocols (from top to bottom, respectively). Images were scaled at equal contrast intensities



Efforts to characterise and harmonise  $^{89}\text{Zr}$ -PET imaging by means of phantom measurement comparisons among different types of systems to ensure quantitative images have been done by Makris et al. [11]. These efforts have been continued by Kaalep et al. [12]. Other system performance comparisons using  $^{89}\text{Zr}$ -filled phantom studies have been performed by Christian et al. [13] to compare and optimise image quality and phantom sphere (lesion) detectability between systems.

Currently, total body  $^{89}\text{Zr}$  immunoPET imaging can last up to 2 h acquisition at later time points at 6–7 days postinjection (p.i.), using the conventional photomultiplier tube (PMT)-based mCT Biograph PET/CT (from now on referred to as mCT (Siemens Healthineers)), our clinical reference system. The improved performance characteristics of the SiPM-based Biograph Vision PET/CT (from now on referred to as Vision (Siemens Healthineers)) are expected to lead to improved  $^{89}\text{Zr}$  immunoPET image quality, and therefore may allow for a reduction in scan duration to increase patient comfort and throughput, and/or administered radioactivity for reduction of radiation exposure.

This study aimed to investigate the difference in semi-quantitative performance between the mCT and the Vision PET/CT systems in  $^{89}\text{Zr}$  immunoPET imaging. In addition, the effects of acquisition time reduction on semiquantitative imaging parameters and its influence on image quality assessment were evaluated.

## Materials and methods

### Patient population

Patients ( $n = 15$  (5 men, 10 women; age 33–79, mean  $\pm$  SD  $58 \pm 13$  years; weight 52–109, mean  $\pm$  SD  $73 \pm 15$  kg) with cancer with visible [ $^{89}\text{Zr}$ ]mAb PET tracer uptake at day 4 p.i. in at least one tumour lesion were enrolled in this prospective study between June 2018 and February 2020 in case of a referral for an  $^{89}\text{Zr}$  immunoPET acquisition to solve a clinical dilemma [14, 15] or for research purposes (ClinicalTrials.gov identifiers NCT02453984 [16] and NCT04029181 [17]). All patients were scanned on the Vision PET/CT system. Patients ( $n = 5$ ) that underwent the dual acquisition protocol were scanned on both PET/CT systems and gave additional written informed consent after being informed on the study aims, procedures and the additional acquisition of a low-dose CT ( $\sim 1$  mSv). For this purpose, the local medical ethics committee exempted approval without additional procedures (waiver number: METc2017/489).

**Table 1** Tumour lesion median  $\text{SUV}_{\text{max}}$  and  $\text{SUV}_{\text{peak}}$  comparison between both systems (only shown for acquisitions on both PET/CT systems ( $n = 5$ ))

Tissue	Biograph mCT		Biograph Vision	
	$\text{SUV}_{\text{max}}$ median (range)	$\text{SUV}_{\text{peak}}$ median (range)	$\text{SUV}_{\text{max}}$ median (range)	$\text{SUV}_{\text{peak}}$ median (range)
<b>Tumour lesions</b>				
<i>Reconstruction protocol:</i>				
$^{89}\text{Zr}$ -EARL/clinical	12.7 (2.2–27.4)	9.8 (1.8–11.9)	25.6 (7.0–64.1)	11.9 (2.1–14.7)
EARL2	15.5 (2.8–48.3)	10.9 (1.8–18.2)	17.9 (4.1–29.7)	10.7 (1.9–13.7)
EARL1	14.1 (2.4–35.7)	10.3 (1.7–14.4)	15.7 (3.4–22.0)	10.1 (2.0–13.6)

## Imaging protocol

Patients received an intravenous injection of 37 MBq  $^{89}\text{Zr}$ -labelled mAb. PET/CT data were acquired on day 4 p.i. On the Vision PET/CT, a standard low-dose CT scan (an X-ray tube current of 43 mAs, a tube voltage of 100 kV and a spiral pitch factor of 1) was performed from the vertex to the toes and used for attenuation and scatter correction. A consecutive emission PET scan was acquired in listmode at 300 s per bed position (s/bp). In case patients were scanned on the mCT, the acquisition parameters of the low-dose CT were as follows: an X-ray tube current of 99 mAs, a tube voltage of 140 kV and a spiral pitch factor of 1.5. PET/CT imaging on the mCT were also performed in listmode at 300 s/bp.

Subsequently, PET listmode data acquired on the Vision were reprocessed to produce additional sets of sinograms corresponding to 225, 150 and 75 s/bp (scan durations are hereinafter referred to as 100%, 75%, 50% and 25% of the acquisition time mimicking shorter scan durations). For reconstruction of Vision PET images, three different protocols were used for each of the four scan durations. We applied the vendor provided reconstruction protocol

currently used for  $^{18}\text{F}$ FDG imaging, i.e. an ordinary Poisson ordered-subset expectation maximisation (OP-OSEM) 3D-iterative algorithm [18] using 4 iterations, 5 subsets, time-of-flight (ToF) application and resolution modelling, without filtering (hereinafter referred to as the Clinical Vision protocol). In addition, the European Association of Nuclear Medicine (EANM) Research Ltd. (EARL)1 and EARL2 reconstructions [19–21] currently used for quantification of clinically acquired oncological  $^{18}\text{F}$ FDG images were obtained using 3D OP-OSEM with 4 iterations and 5 subsets, ToF, with resolution modelling and a Gaussian filter of 7 mm and 5 mm, respectively (hereinafter referred to as the EARL1 and EARL2 Vision protocols). The resulting image size of the images obtained on the Vision was  $220 \times 220$  with a voxel size of  $3.3 \times 3.3 \times 1.5$  mm.

For PET data acquired on the mCT, also three different reconstruction protocols were used. The clinically preferred multicentre validated  $^{89}\text{Zr}$  PET reconstruction protocol [11, 12] using 3D OP-OSEM with 3 iterations, 21 subsets, ToF, resolution modelling and a Gaussian filter of 8 mm (hereinafter referred to as the  $^{89}\text{Zr}$ -EARL mCT protocol [11]). In addition, images acquired on the mCT were also

**Table 2** Healthy tissue median  $\text{SUV}_{\text{max}}$ ,  $\text{SUV}_{\text{peak}}$  and  $\text{SUV}_{\text{mean}}$  comparison between systems (only shown for acquisitions on both PET/CT systems ( $n=5$ ))

Tissue	Biograph mCT			Biograph Vision		
	$\text{SUV}_{\text{max}}$ median (range)	$\text{SUV}_{\text{peak}}$ median (range)	$\text{SUV}_{\text{mean}}$ median (range)	$\text{SUV}_{\text{max}}$ median (range)	$\text{SUV}_{\text{peak}}$ median (range)	$\text{SUV}_{\text{mean}}$ median (range)
Blood pool						
<i>Reconstruction protocol:</i>						
$^{89}\text{Zr}$ -EARL/clinical	10.7 (4.3–13.7)	7.3 (3.7–10.5)	9.11 (3.7–9.8)	14.7 (11.1–25.4)	7.8 (6.3–12.2)	8.6 (6.9–15.0)
EARL2	12.8 (7.0–18.0)	7.4 (5.3–12.1)	9.7 (5.6–11.4)	9.7 (8.5–18.9)	7.2 (5.8–11.7)	8.2 (6.4–14.6)
EARL1	11.9 (6.6–13.8)	7.1 (5.1–11.7)	9.5 (5.5–12.0)	9.0 (7.1–16.4)	7.0 (5.5–11.4)	7.9 (6.4–14.1)
Kidney cortex						
<i>Reconstruction protocol:</i>						
$^{89}\text{Zr}$ -EARL/clinical	5.9 (3.1–8.7)	5.8 (3.1–6.5)	5.6 (3–6.9)	5.9 (6.6–19.1)	6.9 (4.0–7.8)	6.3 (4.2–9.3)
EARL2	7.6 (3.6–9.7)	5.3 (3.0–6.2)	5.0 (3.1–7.9)	7.8 (5.9–10.2)	6.9 (3.8–8.1)	6.4 (3.9–8.3)
EARL1	6.9 (4.9–9.0)	5.7 (3.9–6.5)	5.8 (3.3–7.7)	7.4 (5.4–13.9)	6.7 (3.7–8.1)	6.4 (3.8–7.7)
Spleen						
<i>Reconstruction protocol:</i>						
$^{89}\text{Zr}$ -EARL/clinical	4.3 (3.6–7.6)	3.6 (3.3–7.5)	3.2 (2.6–7.4)	7.7 (6.6–17.3)	4.3 (4.0–8.6)	4.6 (1.9–9.3)
EARL2	5.2 (2.1–7.8)	3.6 (2.1–7.1)	3.6 (1.8–5.6)	6.0 (4.3–11.5)	4.7 (3.5–8.4)	5.0 (2.4–9.1)
EARL1	4.4 (3.4–7.6)	3.6 (3.2–7.0)	3.3 (3.11–6.0)	5.5 (3.7–10.5)	4.7 (3.4–8.2)	3.3 (3.1–5.0)
Liver						
<i>Reconstruction protocol:</i>						
$^{89}\text{Zr}$ -EARL/clinical	8.6 (8.1–9.8)	6.8 (6.4–8.1)	4.9 (4.3–6.0)	11.9 (10.3–23.0)	6.0 (4.8–8.1)	5.4 (4.0–6.1)
EARL2	11.9 (10.2–14.0)	6.8 (6.1–8.7)	5.2 (4.3–6.2)	9.0 (6.5–13.4)	6.1 (4.7–7.9)	5.3 (4.0–6.1)
EARL1	9.5 (8.2–11.6)	7.0 (6.6–8.8)	4.9 (4.3–6.4)	8.4 (5.7–11.4)	6.0 (4.9–7.8)	5.3 (4.0–6.2)



reconstructed to comply with EARL [ $^{18}\text{F}$ ]FDG imaging settings using 3D OP-OSEM with 3 iterations, 21 subsets, ToF, resolution modelling and a Gaussian filter of 6.5 mm (the EARL1 mCT protocol) and a Gaussian filter of 5 mm (the EARL2 mCT protocol). The resulting image size of the images obtained using the mCT was  $256 \times 256$  with a voxel size of  $3.2 \times 3.2 \times 2.0$  mm, thus closely matching the image voxel sizes between systems.

### Semiquantitative image analysis

Reconstructed PET/CT data were semiquantitatively analysed using the quAntitative onCology moleCulaR Analysis suiTE (ACCURATE) version v08072019 [22]. Per image, individual tumour lesions were manually delineated to obtain the maximum and the peak standardised uptake value ( $\text{SUV}_{\text{max}}$  and  $\text{SUV}_{\text{peak}}$ ) of the tumour. In addition, 1-cm-diameter spherical volumes of interest (VOIs) were placed in healthy tissues: blood pool, kidney cortex and spleen well within the boundaries of the organ to avoid partial volume effects. From these VOIs,  $\text{SUV}_{\text{max}}$ ,  $\text{SUV}_{\text{peak}}$  and mean standardised uptake value ( $\text{SUV}_{\text{mean}}$ ) were obtained. A 3-cm-diameter spherical VOI was placed in a homogeneous part of the liver to obtain  $\text{SUV}_{\text{max}}$ ,  $\text{SUV}_{\text{peak}}$  and  $\text{SUV}_{\text{mean}}$ , and to characterise image noise using the standard deviation of the activity within the VOI with regard to the mean activity within the VOI.

### Qualitative image analysis

Images obtained on the Vision at the four different reconstructed scan durations using three different reconstruction protocols were evaluated on image quality. Two nuclear medicine physicians (AHB and WN, with 20 and 5 years of experience in  $^{89}\text{Zr}$  immunoPET image reading, respectively) independently assessed the images using a dedicated *syngo.via* VB30 (Siemens Healthineers) workstation. All images were scored based on a 5-point Likert scale regarding image noise, lesion margin demarcation and overall image quality (see Supplemental Fig. 1 for the used visual image assessment form).

### Statistical analysis

Statistical analyses were performed in SPSS Statistics, version 25.0 (IBM Corp.). To evaluate the difference in semiquantitative performance between systems, non-parametric Wilcoxon signed rank tests were conducted. The difference in lesion  $\text{SUV}_{\text{max}}$  and  $\text{SUV}_{\text{peak}}$  and the difference in healthy tissue  $\text{SUV}_{\text{max}}$ ,  $\text{SUV}_{\text{peak}}$  and  $\text{SUV}_{\text{mean}}$  between systems were explored.

For each reconstruction method performed to obtain images on the Vision, lesion  $\text{SUV}_{\text{max}}$  and  $\text{SUV}_{\text{peak}}$  per scan duration, 75%, 50% and 25%, were compared with the

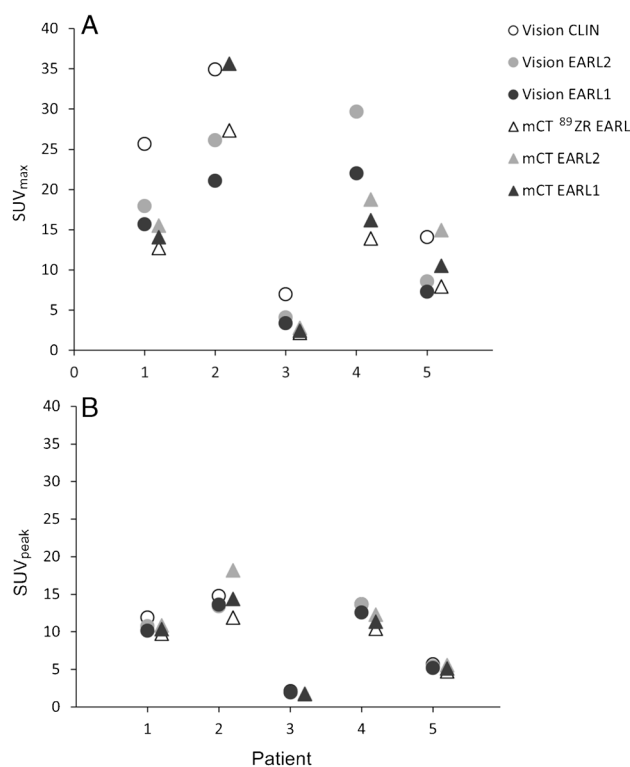


**Fig. 2** Semiquantitative tumour lesion comparison between PET/CT systems. For each patient ( $n=5$ ), the lesion  $\text{SUV}_{\text{max}}$  (A) and  $\text{SUV}_{\text{peak}}$  (B) derived from images obtained with the Vision PET/CT system and using the Clinical Vision (Vision CLIN) (white dot), the EARL2 Vision (grey dot) and the EARL1 Vision reconstruction protocol (black dot) are compared directly with tumour lesion SUVs derived from images using the mCT PET/CT system and  $^{89}\text{Zr}$ -EARL mCT, EARL2 mCT and EARL1 mCT reconstruction protocols (white, grey and black triangles, respectively). Please note, for readability reasons, the tumour lesion  $\text{SUV}_{\text{max}}$  outliers found in patient 4 of 64.1 obtained using the Clinical Vision protocol and of patient 2 of 48.3 obtained using the EARL2 mCT protocol are not shown in subfigure A

lesion  $\text{SUV}_{\text{max}}$  and  $\text{SUV}_{\text{peak}}$  of images acquired at 100% of the count time. A repeated-measures analysis of variance (ANOVA) with post hoc Bonferroni adjustment for pairwise comparison was used. A  $P$  value of less than 0.05 was considered significant. This comparison was also performed for assessing the difference in healthy tissue  $\text{SUV}_{\text{max}}$ ,  $\text{SUV}_{\text{peak}}$  and  $\text{SUV}_{\text{mean}}$  between the 100% scan time images and images acquired at shorter scan durations.

Furthermore, the standard deviation of the voxel values within the liver VOIs was compared between the 100% scan time images and images acquired at shorter scan durations as well.

Inter-reader agreement concerning image noise, tumour lesion demarcation and overall image quality was analysed using kappa statistic. To this aim, the original 5-point scores were reassigned to 2-point scores: 1 + 2 + 3 became 1, and 4 + 5 became 2. A  $P$  value of less than 0.05 was considered significant.

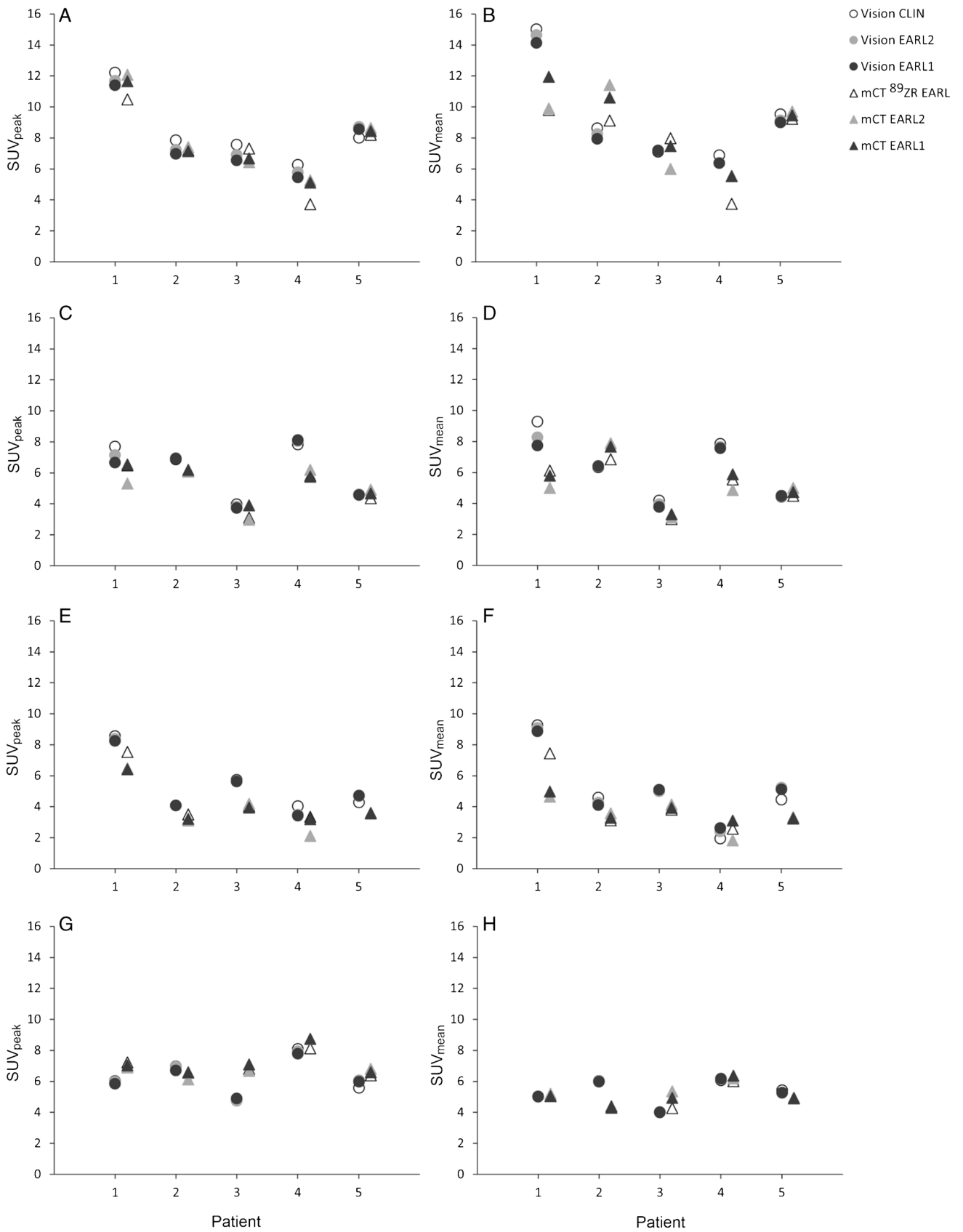


**Fig. 3** Semiquantitative healthy tissue compared between PET/CT systems. For each patient ( $n=5$ ),  $SUV_{peak}$  (left column) and  $SUV_{mean}$  (right column) of healthy tissues (blood pool (A and B), kidney cortex (C and D), spleen (E and F) and liver (G and H)) derived from images obtained through use of the Vision PET/CT system and the Clinical Vision (Vision CLIN) reconstruction protocol (white dot), the EARL2 Vision reconstruction protocol (grey dot) and the EARL1 Vision reconstruction protocol (black dot) are compared directly with healthy tissue SUVs derived from images using the mCT PET/CT system and  $^{89}\text{Zr}$ -EARL mCT, EARL2 mCT and EARL1 mCT reconstruction protocols (white, grey and black triangles, respectively)

## Results

### Semiquantitative image analysis

Five patients were scanned on both PET/CT systems and acquired images were evaluated for the semiquantitative performance comparison of the mCT versus Vision. Each acquisition using the mCT resulted in three images (obtained using three different reconstruction protocols), whereas each acquisition using the Vision resulted in 12 images (three reconstruction methods times four scan durations). For illustrative purposes, Fig. 1 shows example patient PET/CT images acquired using the three reconstruction protocols at different scan durations ranging from 100 to 25%. From top to bottom, Fig. 1 shows images obtained using the Clinical Vision, EARL2 Vision and EARL1 Vision reconstruction protocol, arranged by amount of applied smoothing from least to most. In the Clinical Vision images obtained using 100% scan duration, a clearly demarcated lesion in the vertebra is visible; however, the image has a noisy (speckly) outlook which becomes more disturbing towards shorter acquisition times. The images reconstructed according to EARL2 Vision settings show a sharply demarcated lesion and, because of the applied 5-mm Gaussian filter, the noise is smoothed away which prevents the speckly noise appearance to take the upper hand, also in the images obtained with shorter scan durations. The EARL1 Vision reconstructed images still clearly show the lesion in the vertebra, however apart from smoothing away the noise, the 7 mm Gaussian filter also smooths the edges of the lesion causing a slightly blurred demarcation. Regarding shorter scan durations, the EARL1 reconstructed images show the highest robustness to noise with the least increase in speckly noise pattern towards shorter acquisition times.

For each of the five patients scanned on both the mCT and Vision, a total of 15 images were obtained, whereas 12 images were obtained for each of the 10 patients undergoing acquisition on the Vision only. Overall, 195 images were collected and tumour segmentations were performed on each of the images individually. A total of 5 tumour lesions were found in the double scans, a single lesion per patient. The lesions were first identified on the images acquired on the mCT, our clinical reference system, and subsequently

confirmed on the Vision images. Furthermore, 17 tumour lesions were included in the single acquisitions obtained using the Vision PET/CT (a total of 2 tumour lesions per tissue type per patient). In total, 279 tumour segmentations were made (a segmentation for each reconstruction method and acquisition time resulted for the acquisitions on the mCT in three segmentations per lesion (i.e.  $5 \times 3$  tumour segmentations), and for the Vision in 12 segmentations per lesion (i.e.  $(17 + 5) \times 12$  tumour segmentations).

Concerning the double acquired scans, median lesion  $SUV_{max}$  and  $SUV_{peak}$  derived from the images obtained using the mCT and the EARL standard 1 compliant harmonised reconstruction protocol were 14.1 (range 2.4–35.7) and 10.3 (range 1.7–14.4). For the dual images obtained with the Vision, median lesion  $SUV_{max}$  and  $SUV_{peak}$  derived from images reconstructed according to the EARL1 standard compliant protocol were 17.9 (range 4.1–29.7) and 10.1 (range 2.0–13.6), respectively. An overview of median lesion  $SUV_{max}$  and  $SUV_{peak}$  comparison between PET/CT systems obtained using different reconstruction protocols can be found in Table 1. Regarding the included healthy tissues, a comparison of semiquantitative parameters between PET/CT systems is shown in Table 2.

Scatter plots in Fig. 2 show the difference in lesion  $SUV_{max}$  and  $SUV_{peak}$  between images derived from both PET/CT systems. For each of the healthy tissues, a similar comparison between systems was performed using  $SUV_{max}$ ,  $SUV_{peak}$  and  $SUV_{mean}$  (see Fig. 3). The results from the semiquantitative performance comparison between PET/CT systems using Wilcoxon signed rank tests are shown in Table 3; no significant difference is indicated with 'equivalent'. A significant difference in lesion  $SUV_{max}$  and  $SUV_{peak}$  was found between systems when comparing the images obtained using the Clinical Vision protocol and the  $^{89}\text{Zr}$ -EARL mCT protocol ( $Z = -2.02$ ,  $P < 0.05$ ); no significant differences in tumour lesion  $SUV_{max}$  and  $SUV_{peak}$  were found when comparing system semiquantitative performance using the EARL standard compliant settings 1 and 2. Concerning the healthy tissues, significantly different  $SUV_{max}$  were found between systems in the blood pool, kidney cortex, spleen and liver when using the Clinical Vision and  $^{89}\text{Zr}$ -EARL mCT reconstruction protocol ( $P < 0.05$ ). Using these reconstruction settings,  $SUV_{peak}$  measured in the kidney cortex differed significantly between systems as well ( $Z = -2.02$ ,  $P < 0.05$ ). No significant differences in healthy tissue  $SUV_{max}$ ,  $SUV_{peak}$  and  $SUV_{mean}$  were found when comparing system semiquantitative performance using the EARL standard compliant settings 1 and 2 for the blood pool, kidney cortex and liver. However, for the spleen, significant differences between systems regardless of reconstruction settings and semiquantitative parameters were observed ( $P < 0.05$ ). Table 2 shows an overall increase of approximately 25% in median SUV for the spleen irrespective of reconstruction protocol.



**Table 3** Semiquantitative performance in tumour lesion comparison between both PET/CT systems ( $n=5$ ) using the Wilcoxon signed rank test

	Z	P value	Equivalence
<b>Tumour lesions</b>			
<i>Reconstruction protocol:</i>			
<sup>89</sup> Zr-EARL/clinical			
SUV <sub>max</sub>	-2.02	0.04	No
SUV <sub>peak</sub>	-2.02	0.04	No
EARL2			
SUV <sub>max</sub>	-0.14	0.89	Yes
SUV <sub>peak</sub>	-0.67	0.50	Yes
EARL1			
SUV <sub>max</sub>	-0.14	0.89	Yes
SUV <sub>peak</sub>	-0.41	0.69	Yes

Boxplots in Fig. 4 show lesion SUV<sub>max</sub> and SUV<sub>peak</sub> comparisons between different scan durations derived from images obtained using the Vision. A significant difference was found in lesion SUV<sub>max</sub> between images using the Clinical Vision reconstruction protocol obtained at 100% scan duration and 25% ( $P=0.009$ , 95% CI (-18.0 to -2.0)), and between images obtained at 75% scan duration and 25% ( $P=0.008$ , 95% CI (-17.1 to -2.0)). When using the EARL2 Vision reconstruction settings, lesion SUV<sub>max</sub> differed significantly between 75 and 25% scan duration ( $P=0.02$ , 95% CI (-5.5 to -0.3)). Images reconstructed using the EARL1 Vision protocol showed significant differences in lesion SUV<sub>max</sub> between 100 and 25% scan duration ( $P=0.001$ , 95% CI (-2.3 to -0.5)), and between 75 and 25% ( $P=0.009$ , 95% CI (-2.5 to -0.3)). No significant differences were found in lesion SUV<sub>peak</sub> between images obtained at different scan durations.

The results of the healthy tissue comparisons between scan durations are shown in Fig. 5. No significant differences in healthy tissue SUV<sub>mean</sub> and SUV<sub>peak</sub> were found between images obtained using the Vision at different scan durations. Because of different <sup>89</sup>Zr-labelled mAbs used in this study, a substantial visual difference was observed in the uptake in the spleen. For clarity, the healthy tissue comparisons per <sup>89</sup>Zr-labelled mAb for the spleen are shown in Supplemental Fig. 2.

Noise estimates from calculation of the coefficient of variation (COV) derived from the 3-cm-diameter liver VOIs in each image are shown in Fig. 6. A difference in image noise levels can be observed between reconstruction methods and scan durations. Noise levels increase with shorter scan times; this effect is more prominent when using the Clinical Vision reconstruction protocol compared to EARL2 and EARL1 compliant reconstruction settings.

## Qualitative image analysis

Vision only images ( $n=15$  patients) were reconstructed using three different reconstruction protocols and visually assessed on noise levels, lesion demarcation and overall image quality. Highest mean scores on noise levels and overall image quality were assigned to the images reconstructed according to the EARL1 Vision protocol (mean scores on noise and image quality of 4.3 and 4.4 at 100% of the scan duration, 3.6 and 3.9 at 75% and 3.1 and 3.3 at 50%, respectively). The EARL2 Vision reconstructed images received a slightly higher appreciation on lesion demarcation with respect to the EARL1 Vision reconstructed images (mean score of 4.4 versus 4.2 at 100% of the scan duration, 4.1 versus 3.9 at 75% and 3.7 versus 3.5 at 50%).

Inter-reader agreement ranged from fair to moderate on noise, lesion demarcation and overall image quality with  $\kappa = 0.23$  ( $P=0.000$ , 95% CI (0.12–0.34)),  $\kappa = 0.27$  ( $P=0.000$ , 95% CI (0.13–0.41)) and  $\kappa = 0.41$  ( $P=0.000$ , 95% CI (0.28–0.55)), respectively.

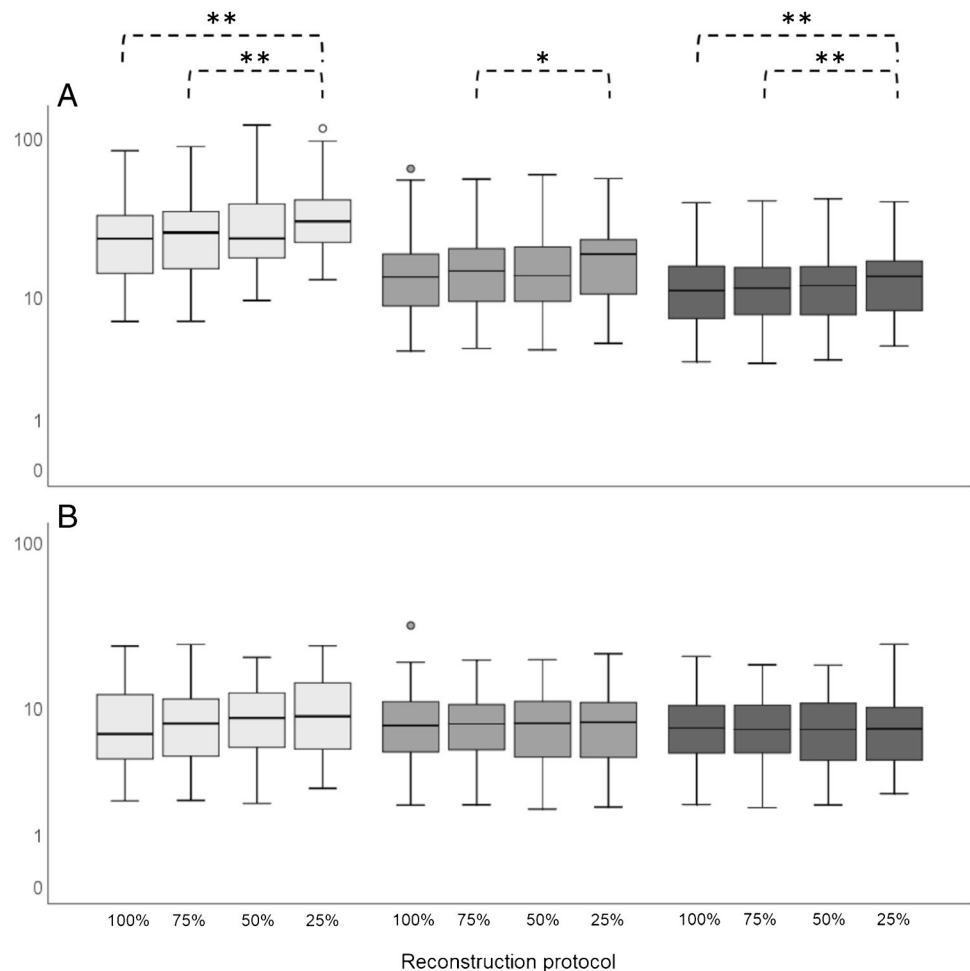
## Discussion

In the current study, semiquantitative performance of the Vision with regard to its predecessor, the mCT, was evaluated for <sup>89</sup>Zr immunoPET imaging in oncology patients. In addition, possibilities of reducing scan time while maintaining image quality using the Vision were explored.

This study shows that when using the Vision PET/CT system, a reduction in scan time of 50% is possible regardless of reconstruction settings according to Fig. 4. However, the use of images reconstructed according to EARL2 Vision or the Clinical Vision protocol would result in too much elevated noise levels (see Fig. 6). Therefore, we recommend to apply the EARL1 Vision settings for image reconstruction for a 50% reduction in scan duration while maintaining semiquantitative PET image accuracy.

Significant differences in semiquantitative PET image parameters were found for shorter scan durations when using the Clinical Vision reconstruction protocol, especially SUV<sub>max</sub> increases at shorter scan times (50% and 25%) with regard to 100% acquisition time. A non-negligible consideration when using SUV<sub>max</sub> for uptake measurements in PET images is statistical quality. When reducing scan time, variability in SUV<sub>max</sub> can largely be explained by the associated increase in noise [23] (see Fig. 6). The addition of a Gaussian filter (as used in the EARL2 and EARL1 Vision reconstruction settings (7 mm and 5 mm, respectively)) smooths the image hereby reducing noise and SUV<sub>max</sub> variability [24] which results in similar results for lesion quantification at shorter scan times.

**Fig. 4** Vision only semiquantitative tumour lesion comparison. For all patients ( $n = 15$ ), the tumour lesion  $SUV_{max}$  (A) and  $SUV_{peak}$  (B) derived from images obtained using the Vision PET/CT system and the Clinical Vision reconstruction protocol (light grey), the EARL2 Vision reconstruction protocol (grey) and the EARL1 Vision reconstruction protocol (dark grey) are compared at different scan durations (100 to 25%, from left to right for each reconstruction protocol). The boxes bound the interquartile range (IQR) divided by the median SUV. The whiskers extend to a maximum of  $1.5 \times IQR$  beyond the box. \* indicates  $P < 0.05$  and \*\* indicates  $P < 0.01$ . Outliers are represented by dots



A more robust alternative, and diminishing the need for a filter at shorter acquisition times, is to use  $SUV_{peak}$  for lesion quantification. Although  $SUV_{peak}$  is expected to be more susceptible to partial volume effect in small lesion segmentation (19), its semiquantitative performance is less affected by scan duration and reconstruction protocol (see Figs. 4 and 5). Makris et al. [11] previously recommended the use of  $SUV_{peak}$  for performing semiquantitatively accurate  $^{89}Zr$  immunoPET imaging studies. They found very low variability in  $SUV_{peak}$  between various PET/CT systems and imaging sites. Moreover, this recommendation has then been affirmed in an  $^{89}Zr$  immunoPET imaging study by Kaalep et al. [12] describing a multicentre PET/CT system and reconstruction comparison trial in which  $SUV_{peak}$  was found to be least sensitive to noise and reconstruction differences. As we also found  $SUV_{max}$  to vary not only between reconstructed images obtained from different PET/CT systems, but also between differently reconstructed images obtained from a single system, our recommendation is (in line with previously reported results described above) to use  $SUV_{peak}$  for quantification of  $^{89}Zr$  immunoPET images. In case EARL standard 1 compliant settings are used (for comparison

between systems),  $SUV_{max}$  could be reported as well for lesion quantification besides  $SUV_{peak}$ .

In order to obtain quantitatively comparable results, we standardise and harmonise PET imaging procedures [19] incorporating various methods, including different amounts of applied smoothing. With the introduction of new PET systems with improved performance characteristics, the harmonisation and standardisation specifications are updated as well [20] to preserve some of the improved image quality that can be obtained. However, in the case of  $^{89}Zr$  immunoPET imaging, only a low amount of activity can be administered (37 MBq) due to the long half-life associated with high radiation exposure. This low amount of activity in addition to the low positron abundance causes image quality of  $^{89}Zr$  immunoPET images to be in the bottom range; low count statistics result in overall poor image quality. Hence, reconstruction protocols that smooth in excess, such as incorporated in the EARL1 compliant reconstruction settings, are still required under these circumstances.

In the current study, the difference between  $SUV_{peak}$  and  $SUV_{mean}$  derived from healthy tissues is minimal due to the small 1-cm-diameter spherical VOI that

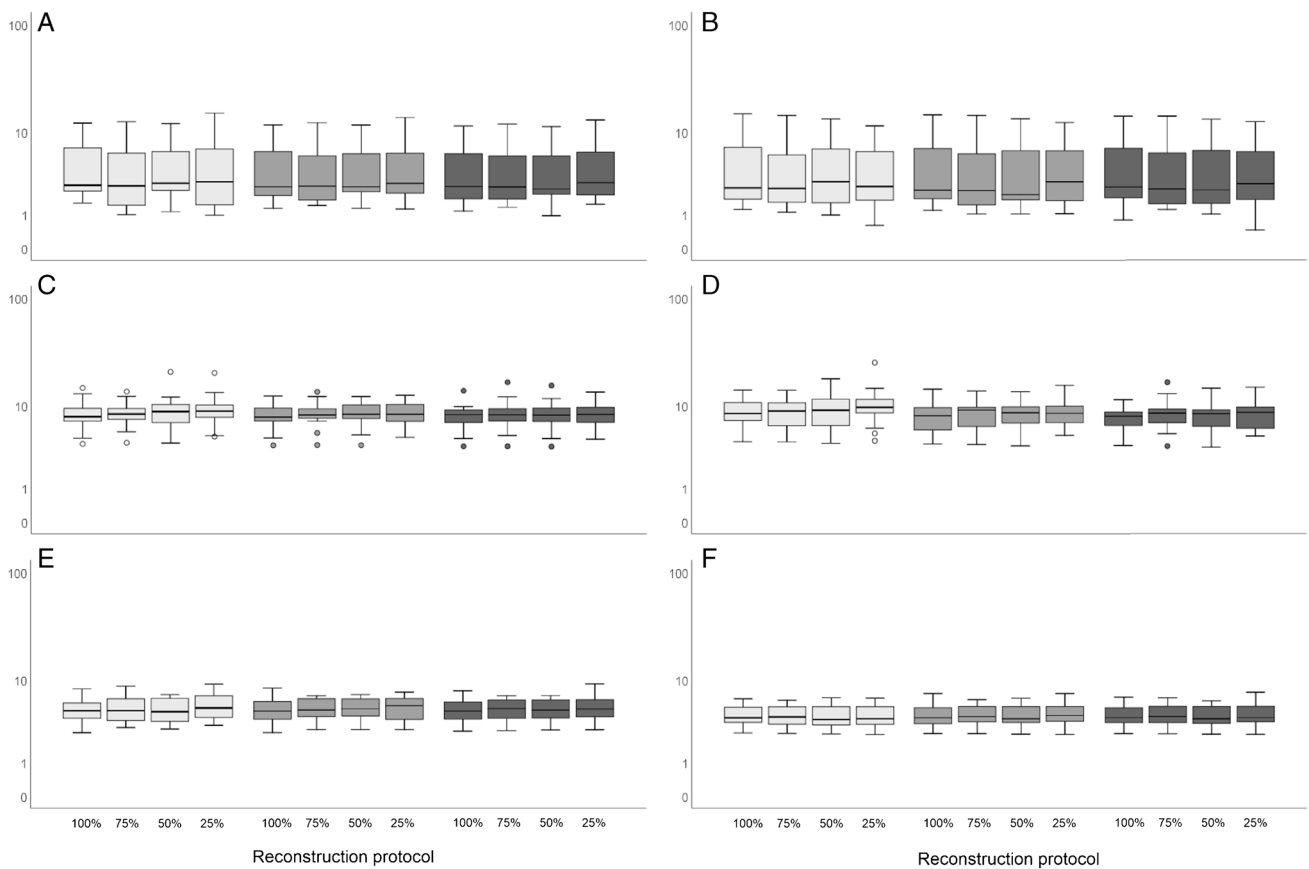


**Fig. 5** Vision only semiquantitative healthy tissue comparison between scan durations. For all patients ( $n=15$ ),  $SUV_{peak}$  (left column) and  $SUV_{mean}$  (right column) of healthy tissues (blood pool (A and B), kidney cortex (C and D), spleen (E and F) and liver (G and H)) derived from images obtained through use of the Vision PET/CT

system and the Clinical Vision reconstruction protocol (light grey), the EARL2 Vision reconstruction protocol (grey) and the EARL1 Vision reconstruction protocol (dark grey) are compared at different scan durations (100 to 25%, from left to right for each reconstruction protocol)

was used in the blood pool, kidney cortex and spleen.  $SUV_{mean}$  was included in the evaluation of semiquantitative performance comparison of healthy tissues between

systems as  $SUV_{mean}$  measurement of these organs is used, for example, in whole organ dosimetry analyses. Using  $SUV_{mean}$  for whole organ dosimetry avoids susceptibility

**Fig. 6** Liver COV ( $n=15$ ) obtained from the Clinical Vision (light grey), EARL2 Vision (grey) and EARL1 Vision compliant (dark grey) reconstructed images at 100%, 75%, 50% and 25% of the scan time (from left to right)

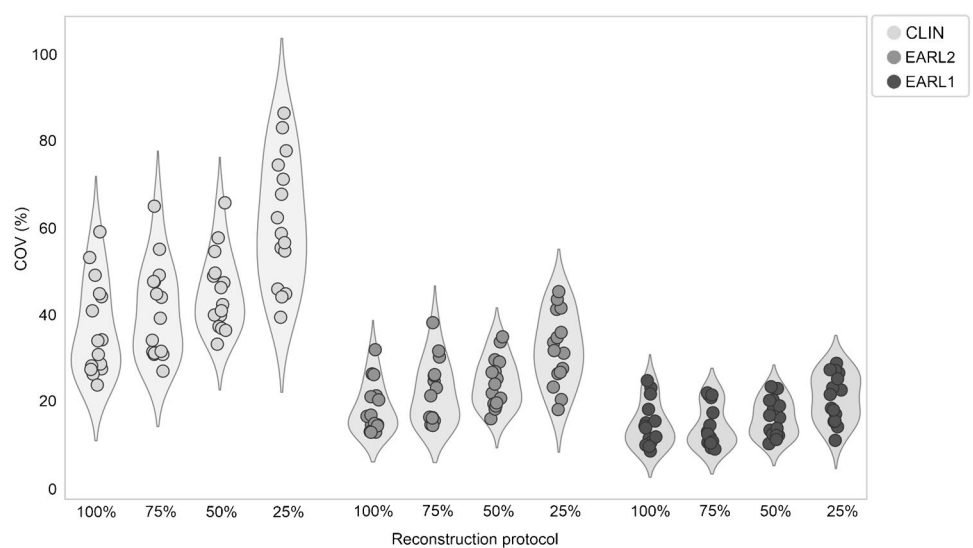


**Table 4** Quantitative performance in healthy tissue comparison between systems ( $n=5$ ) using the Wilcoxon signed rank test

	Z	Pvalue	Equivalence
<b>Healthy tissues</b>			
Blood pool			
<i>Reconstruction protocol:</i>			
<sup>89</sup> Zr-EARL/clinical			
SUV <sub>max</sub>	-2.02	0.04	No
SUV <sub>peak</sub>	-1.75	0.08	Yes
SUV <sub>mean</sub>	-0.67	0.50	Yes
EARL2			
SUV <sub>max</sub>	-0.14	0.89	Yes
SUV <sub>peak</sub>	-0.67	0.50	Yes
SUV <sub>mean</sub>	-0.67	0.50	Yes
EARL1			
SUV <sub>max</sub>	-0.67	0.50	Yes
SUV <sub>peak</sub>	-0.41	0.69	Yes
SUV <sub>mean</sub>	-0.14	0.89	Yes
Kidney cortex			
<i>Reconstruction protocol:</i>			
<sup>89</sup> Zr-EARL/clinical			
SUV <sub>max</sub>	-2.02	0.04	No
SUV <sub>peak</sub>	-2.02	0.04	No
SUV <sub>mean</sub>	-1.21	0.23	Yes
EARL2			
SUV <sub>max</sub>	-1.21	0.23	Yes
SUV <sub>peak</sub>	-1.75	0.08	Yes
SUV <sub>mean</sub>	-0.94	0.35	Yes
EARL1			
SUV <sub>max</sub>	-1.21	0.23	Yes
SUV <sub>peak</sub>	-0.94	0.35	Yes
SUV <sub>mean</sub>	-0.94	0.35	Yes
Spleen			
<i>Reconstruction protocol:</i>			
<sup>89</sup> Zr-EARL/clinical			
SUV <sub>max</sub>	-2.02	0.04	No
SUV <sub>peak</sub>	-2.02	0.04	No
SUV <sub>mean</sub>	-1.75	0.08	Yes
EARL2			
SUV <sub>max</sub>	-1.48	0.14	Yes
SUV <sub>peak</sub>	-2.02	0.04	No
SUV <sub>mean</sub>	-2.02	0.04	No
EARL1			
SUV <sub>max</sub>	-2.02	0.04	No
SUV <sub>peak</sub>	-2.02	0.04	No
SUV <sub>mean</sub>	-1.75	0.08	Yes
<b>Liver</b>			
<i>Reconstruction protocol:</i>			
<sup>89</sup> Zr-EARL/clinical			
SUV <sub>max</sub>	-2.02	0.04	No
SUV <sub>peak</sub>	-1.48	0.14	Yes
SUV <sub>mean</sub>	-0.67	0.50	Yes
EARL2			
SUV <sub>max</sub>	-1.21	0.23	Yes

**Table 4** (continued)

	Z	Pvalue	Equivalence
SUV <sub>peak</sub>	-1.21	0.23	Yes
SUV <sub>mean</sub>	-0.14	0.89	Yes
EARL1			
SUV <sub>max</sub>	-0.94	0.35	Yes
SUV <sub>peak</sub>	-1.75	0.08	Yes
SUV <sub>mean</sub>	-0.14	0.89	Yes

to segmentation variability as opposed to using SUV<sub>max</sub> or SUV<sub>peak</sub> [25]. Please note, the significant difference in SUV<sub>max</sub> for tumour lesions and all healthy tissues found between systems using the Clinical Vision reconstruction protocol versus the <sup>89</sup>Zr-EARL mCT protocol (see Tables 3 and 4). This difference can be explained by the 8-mm Gaussian smoothing filter applied to the images acquired using the mCT, whereas images acquired on the Vision were not smoothed at all. With regard to semiquantitative performance between systems at 100% acquisition time, no further significant differences between tumour lesions and blood pool, kidney cortex and liver measurements were found. For the spleen however, a significant increase in SUV measured on the images obtained from the Vision PET/CT was observed with respect to the images obtained from the mCT PET/CT. This was only the case for the spleen (and not for the other healthy tissues). Thus far, we have not found a plausible explanation. We suspect the improved tissue demarcation due to improved sensitivity and ToF on the Vision PET/CT system could play a role here. No patient instructions with respect to food and fluid intake prior to <sup>89</sup>Zr immunoPET acquisition were given, resulting in large cold areas with the size of a filled stomach on the acquired images. These cold spots were more prominently visible on the Vision images with a clearer demarcation of the stomach. Due to the improved ToF, better contrast recovery in the spleen using the Vision PET/CT may have resulted in a better reflection of the true counts originating from the spleen as opposed to some possible larger signal spill over between the cold stomach and the very intense spleen on the mCT images. Future <sup>89</sup>Zr immunoPET studies with a larger homogeneous patient population will have to explore this phenomenon to clarify these findings. Until then, the spleen should not be used as reference tissue in <sup>89</sup>Zr immunoPET imaging studies.

Regarding qualitative image assessment, overall, the images reconstructed according to the EARL1 protocol received the highest scores resulting from the visual assessment; higher mean scores were obtained for noise levels and overall image quality, and there was only a slight difference in lesion demarcation scores in favour of the EARL2 reconstructed images. Furthermore, fair to moderate inter-reader

agreement was achieved. As the nuclear medicine physicians were asked to score the images individually without a direct comparison with optimal  $^{89}\text{Zr}$  immunoPET image quality, scoring was considered difficult. Another factor that should be considered when interpreting these results is that the image quality of [ $^{18}\text{F}$ ]FDG PET/CT scans (compared to  $^{89}\text{Zr}$  PET/CT images) on the Vision is excellent. These excellent [ $^{18}\text{F}$ ]FDG PET images might have been an unintentional reference for visual  $^{89}\text{Zr}$  immunoPET image assessment. Furthermore, previous experience with  $^{89}\text{Zr}$  immunoPET readings, and personal preference of the reading Nuclear Medicine physicians regarding acceptable image quality could have played a role in the observed variation in the image quality assessment.

Previous work also performed by our research group explored the effect of scan time reduction on semiquantitative PET image parameters and image quality in [ $^{18}\text{F}$ ]FDG PET imaging using the Vision [4]. Here, a factor 3 reduction in scan time was considered possible while maintaining image quality using the clinically preferred Vision reconstruction protocol with additional 2-mm Gaussian filtering. In the current study, possibilities to reduce scan duration in  $^{89}\text{Zr}$  immunoPET imaging were explored. Using the EARL Vision protocols, semiquantitative performance remains reliable when decreasing scan duration up to a factor of 2 (see Figs. 4 and 5) at the cost of a slight increase in noise (see Fig. 6). Therefore, for  $^{89}\text{Zr}$  immunoPET imaging in the clinic using an SiPM-based PET/CT, one may choose to reduce scan duration to improve patient comfort and increase throughput. On the other hand, in case of paediatric patients or for non-life-threatening diseases, an equally proportional reduction in the amount of injected activity would be recommended to reduce radiation exposure. However, as shown before for [ $^{18}\text{F}$ ]FDG PET studies [4], more room for optimising image quality by changing amount of administered activity and/or scan duration is feasible because of the higher positron abundance and typically higher injected activities allowed from a radiation safety perspective.

## Conclusion

In this study, we found, when using the SiPM-based Vision PET/CT for  $^{89}\text{Zr}$  immunoPET imaging and the EARL standard 1 compliant reconstruction settings, semiquantitative PET image parameters to remain reliable when using images obtained at reduced scan durations up to a factor of 2 compared to using the conventional PMT-based mCT PET/CT system.

Also, as  $\text{SUV}_{\text{max}}$  is highly affected by noise and reconstruction settings, and differs considerably in quantification of tumour lesions as well as healthy tissues between various PET/CT systems, we strongly recommend using the EARL

standard 1 compliant reconstruction protocol and to report  $\text{SUV}_{\text{peak}}$  for reliable, comparable across systems, tumour lesion quantification in  $^{89}\text{Zr}$  PET/CT imaging.

**Supplementary Information** The online version contains supplementary material available at <https://doi.org/10.1007/s00259-023-06194-4>.

**Author contribution** The manuscript has been read and approved for submission by all the named authors: JS, AB and RB contributed to the conception and design. JS, AB, WN, LR, PD and EV contributed to the data generation. JS, EE, DC, RB, AB and WN contributed to data analysis and interpretation. JS, RB, AB and WN contributed to the manuscript preparation. JS, AB, RB, WN, RD, LR, PD and EV contributed to the manuscript review and editing.

**Data availability** The datasets generated and analysed during the current study are not publicly available due to sensitive information, but could be made available in anonymous form from the corresponding author on reasonable request.

## Declarations

**Ethical approval** This study was performed in line with the principles of the Declaration of Helsinki. The medical ethics committee of the University Medical Centre Groningen exempted approval without additional procedures (waiver number: METc2017/489).

**Consent to participate** All patients that underwent the dual acquisition protocol were scanned on both PET/CT systems and gave additional written informed consent after being informed on the study aims and procedures.

**Competing interests** The authors declare no competing interests.

**Open Access** This article is licensed under a Creative Commons Attribution 4.0 International License, which permits use, sharing, adaptation, distribution and reproduction in any medium or format, as long as you give appropriate credit to the original author(s) and the source, provide a link to the Creative Commons licence, and indicate if changes were made. The images or other third party material in this article are included in the article's Creative Commons licence, unless indicated otherwise in a credit line to the material. If material is not included in the article's Creative Commons licence and your intended use is not permitted by statutory regulation or exceeds the permitted use, you will need to obtain permission directly from the copyright holder. To view a copy of this licence, visit <http://creativecommons.org/licenses/by/4.0/>.

## References

1. López-Mora DA, Flotats A, Fuentes-Ocampo F, Camacho V, Fernández A, Ruiz A, et al. 2019 Comparison of image quality and lesion detection between digital and analog PET/CT. *Eur J Nucl Med Mol Imaging. European Journal of Nuclear Medicine and Molecular Imaging.* 46:1383–90.
2. van Sluis J, Boellaard R, Somasundaram A, van Snick PH, Borra RJH, Dierckx RAJO, et al. Image quality and semiquantitative measurements on the biograph vision PET/CT system: initial experiences and comparison with the biograph MCT. *J Nucl Med.* 2020;61:129–35.
3. Sonni I, Baratto L, Park S, Hatami N, Srinivas S, Davidzon G, et al. 2018 Initial experience with a SiPM-based PET/CT scanner:



- influence of acquisition time on image quality. *EJNMMI Phys. EJNMMI Physics*;5:9.
4. van Sluis J, Boellaard R, Dierckx RAJO, Stormezand GN, Glaudemans AWJM, Noordzij W. Image quality and activity optimization in oncologic 18F-FDG PET using the digital Biograph Vision PET/CT system. *J Nucl Med.* 2020;61:764–71.
  5. Jauw YWS, Menke-van der Houven van Oordt CW, Hoekstra OS, Hendrikse HN, Vugts DJ, Zijlstra JM, et al. 2016 Immuno-positron emission tomography with zirconium-89-labeled monoclonal antibodies in oncology: what can we learn from initial clinical trials? *Front Pharmacol.* 7:1–15.
  6. Van De Watering FCJ, Rijpkema M, Perk L, Brinkmann U, Oyen WJG, Boerman OC. 2014 Zirconium-89 labeled antibodies: a new tool for molecular imaging in cancer patients. *Biomed Res Int.* 203601.
  7. Zhang Y, Hong H, Cai W. PET tracers based on zirconium-89. *Curr Radiopharm.* 2011;4:131–9.
  8. Verel I, Gerard WM V, Boellaard R, Marijke S-VW, Gordon B S, Guus AMS van D. 2003 BASIC SCIENCE INVESTIGATIONS 89 Zr Immuno-PET: comprehensive procedures for the production of 89 Zr-labeled monoclonal antibodies. *J Nucl Med.* 44:1271–81.
  9. De Feo SM, Pontico M, Frantellizzi V, Corica F, De Cristofaro F, De Vincentis G. Zr - PET imaging in humans : a systematic review. *Clin Transl Imaging Springer International Publishing.* 2022;10:23–36.
  10. Conti M, Eriksson L. Physics of pure and non-pure positron emitters for PET: a review and a discussion. *EJNMMI Phys EJNMMI Physics.* 2016;3:3–8.
  11. Makris NE, Boellaard R, Visser EP, De Jong JR, Vanderlinden B, Wiertz R, et al. Multicenter harmonization of 89Zr PET/CT performance. *J Nucl Med.* 2014;55:264–7.
  12. Kaalep A, Huisman M, Sera T, Vugts D, Boellaard R. 2018 Feasibility of PET/CT system performance harmonisation for quantitative multicentre 89Zr studies. *EJNMMI Phys. EJNMMI Physics*; 5:26.
  13. Christian PE, Williams SP, Burrell L, Castaneda P, Albiani J, Sandella N, et al. Optimization of 89Zr PET imaging for improved multisite quantification and lesion detection using an anthropomorphic phantom. *J Nucl Med Technol.* 2020;48:5457.
  14. Bensch F, Brouwers AH, Lub-de Hooge MN, de Jong JR, van der Vegt B, Sleijfer S, et al. 2018 89Zr-trastuzumab PET supports clinical decision making in breast cancer patients, when HER2 status cannot be determined by standard work up. *Eur J Nucl Med Mol Imaging. European Journal of Nuclear Medicine and Molecular Imaging*; 45:2300–6.
  15. Dijkers EC, Oude Munnink TH, Kosterink JG, Brouwers AH, Jager PL, de Jong JR, et al. Biodistribution of 89Zr-trastuzumab and PET imaging of HER2-positive lesions in patients with metastatic breast cancer. *Clin Pharmacol.* 2010;87:586–92.
  16. Bensch F, van der Veen EL, Lub-de Hooge MN, Jorritsma-Smit A, Boellaard R, Kok IC, et al. 89Zr-atezolizumab imaging as a non-invasive approach to assess clinical response to PD-L1 blockade in cancer. *Nat Med.* 2018;24:1852–8.
  17. Kist de Ruijter L, van de Donk PP, Hooiveld-Noeken JS, Giesen D, Elias SG, Lub-de Hooge MN, et al. 2022 Whole-body CD8+ T cell visualization before and during cancer immunotherapy: a phase 1/2 trial. *Nat Med.* 28:2601–10.
  18. Varrone A, Sjöholm N, Eriksson L, Gulyás B, Halldin C, Farde L. Advancement in PET quantification using 3D-OP-OSEM point spread function reconstruction with the HRRT. *Eur J Nucl Med Mol Imaging.* 2009;36:1639–50.
  19. Boellaard R, Delgado-Bolton R, Oyen WJG, Giammarile F, Tatsch K, Eschner W, et al. 2014 FDG PET/CT: EANM procedure guidelines for tumour imaging: version 2.0. *Eur J Nucl Med Mol Imaging.* 42:328–54.
  20. Boellaard R. New developments of EANM oncology PET/CT guidelines and update of the EARL accreditation standards presentation. 2018. Available from: [https://eanm-earl-wordpress.es.net/wp-content/uploads/2021/04/EARL\\_18F\\_stds2\\_PPP\\_Boellaard\\_Oct2018-1.pdf](https://eanm-earl-wordpress.es.net/wp-content/uploads/2021/04/EARL_18F_stds2_PPP_Boellaard_Oct2018-1.pdf). Accessed February 2023.
  21. Kaalep A, Burggraaff CN, Pieplensbosch S, Verwer EE, Sera T, Zijlstra J, et al. Quantitative implications of the updated EARL 2019 PET–CT performance standards. *EJNMMI Phys EJNMMI Physics.* 2019;6:1–16.
  22. Boellaard R. 2018 Quantitative oncology molecular analysis suite: ACCURATE. *J Nucl Med. Society of Nuclear Medicine*; [Abstract] 59:1753–1753.
  23. Lodge MA, Chaudhry MA, Wahl RL. Noise considerations for PET quantification using maximum and peak standardized uptake value. *J Nucl Med.* 2012;53:1041–7.
  24. Boellaard R, Krak NC, Hoekstra OS, Lammertsma AA. Effects of noise, image resolution, and ROI definition on the accuracy of standard uptake values: a simulation study. *J Nucl Med.* 2004;45:1519–27.
  25. Schwartz J, Humm JL, Gonen M, Kalaigian H, Schoder H, Larson SM, et al. Repeatability of SUV measurements in serial PET. *Med Phys.* 2011;38:2629–38.

**Publisher's note** Springer Nature remains neutral with regard to jurisdictional claims in published maps and institutional affiliations.